Title
Correlative Cryogenic Spectromicroscopy to Investigate Selenium Bioreduction Products

Journal
Environmental Science and Technology, 52(2)

ISSN
0013-936X

Authors
Fakra, Sirine C
Luef, Birgit
Castelle, Cindy J
et al.

Publication Date
2018-01-16

DOI
10.1021/acs.est.5b01409

Peer reviewed

Correlative Cryogenic Spectromicroscopy to Investigate Selenium Bioreduction Products

Sirine C. Fakra*†§, Birgit Luef†⊥, Cindy J. Castelle†, Sean W. Mullin†#, Kenneth H. Williams∥, Matthew A. Marcus§, Denise Schichnes‡, and Jillian F. Banfield†∥

†Department of Earth and Planetary Science and ‡Department of Plant & Microbial Biology, University of California, Berkeley, California 94720, United States

§Advanced Light Source and ∥Earth Sciences Division, Lawrence Berkeley National Lab, Berkeley, California 94720, United States

DOI: 10.1021/acs.est.5b01409

*Tel: 510-495-2855; fax: 510-486-4102; e-mail: sfakra@lbl.gov.

Abstract

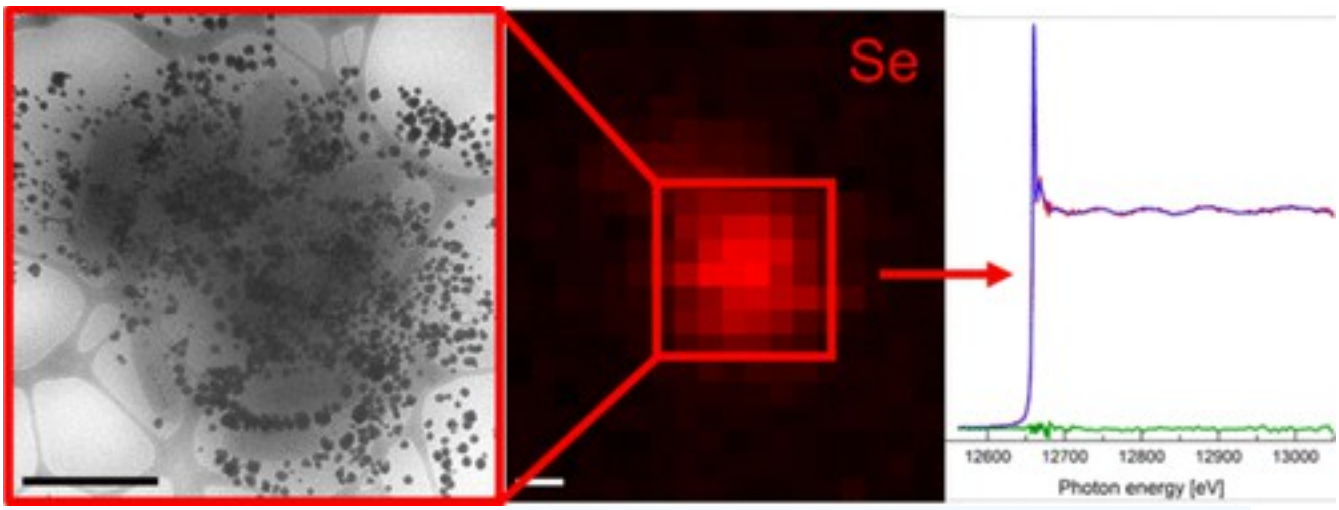

Accurate mapping of the composition and structure of minerals and associated biological materials is critical in geomicrobiology and environmental research. Here, we have developed an apparatus that allows the correlation of cryogenic transmission electron microscopy (cryo-TEM) and synchrotron hard X-ray microprobe (SHXM) data sets to precisely determine the distribution, valence state, and structure of selenium in biofilms sampled from a contaminated aquifer near Rifle, CO. Results were replicated in the laboratory via anaerobic selenate-reducing enrichment cultures. 16S rRNA analyses of field-derived biofilm indicated the dominance of Betaproteobacteria from the Comamonadaceae family and uncultivated members of the *Simplicispira* genus. The major product in field and culture-derived biofilms is ∼25–300 nm red amorphous Se^0 aggregates of colloidal nanoparticles. Correlative analyses of the cultures provided direct evidence for the microbial dissimilatory reduction of Se(VI) to Se(IV) to Se^0. Extended X-ray absorption fine-structure spectroscopy showed red amorphous Se^0 with a first shell Se–Se interatomic distance of 2.339 ± 0.003 Å. Complementary scanning transmission X-ray microscopy revealed that these aggregates are strongly associated with a protein-rich biofilm matrix. These findings have important implications for predicting the

stability and mobility of Se bioremediation products and understanding of Se biogeochemical cycling. The approach, involving the correlation of cryo-SHXM and cryo-TEM data sets from the same specimen area, is broadly applicable to biological and environmental samples.

Introduction

Deciphering the roles of microbial processes in biogeochemical transformations is important for many biomineral systems and environmental research in general. The characterization of field samples is necessary because relevant pure cultures or characterized mixed microbial communities can be difficult to obtain and can miss critical aspects that are key to environmental processes. Damage to biological materials can occur by shrinkage, breakage, or the loss of subcellular and extracellular structures. Furthermore, the examination of dry or freeze-dried samples can lead to denaturation of proteins, alteration of the mineral structure, and loss of spatial resolution at the cell surface–nanoparticle interface, yielding incorrect interpretations.(1)

Most biomineral samples are complex and of variable chemical composition at the nano- and microscales and often contain poorly ordered materials in low concentrations. Synchrotron hard X-ray microprobes (SHXM) are ideally suited to characterize such systems and provide metal distribution through X-ray fluorescence (μXRF) mapping, valence state, and local atomic structure via X-ray absorption spectroscopy (μXAS), and phase identification via X-ray diffraction (μXRD).(2) X-ray damage through metal photoreduction and oxidation and amorphization has been well-documented and is especially acute in organics-containing samples.(3-5) Selenium (Se) compounds in particular are prone to X-ray damage, as illustrated by the breaking of the Cγ–Se bond in selenomethionine (SeMet),(6) selenate photoreduction,(7) and selenite photo-oxidation,(8)or just simply reported, as in the case of Se-contaminated biological wastewater samples.(9)Additionally, organic-bound metals and low-Z-containing molecules are often difficult to analyze at room temperature because thermal vibrations damp the amplitude of extended X-ray absorption fine-structure (EXAFS) oscillations, especially at high photoelectron wavenumbers. These issues are exacerbated in dilute or poorly ordered biominerals, where longer beam exposure is usually required for adequate signal-to-noise ratios. For the alleviation of these effects, measurements are most often carried out at LN_2 (77 K) or less frequently at LHe (4 K) temperatures. In the case of selenium, prior Se K-edge cryo-EXAFS studies of amorphous and crystalline Se(10) demonstrated that the Debye–Waller thermal disorder component is only marginally reduced below 100 K, suggesting that the use

of LHe (versus LN_2) would not significantly improve the EXAFS signal. Lastly, cryogenic analyses should allow better detection of any potentially volatile selenides produced.

There is a strong incentive to link cryogenic SHXM with cryogenic transmission electron microscopy (cryo-TEM).(11) Cryo-TEM provides ultrastructural information at a 2–4 nm resolution(12) on whole frozen hydrated intact bacteria embedded in amorphous (vitreous) ice, eliminating artifacts associated with traditional fixation and dehydration methods or sectioning.(1)The sample is generally cooled with LN_2 (versus LHe(13)), and low-dose imaging mode is used to minimize electron damage and preserve sample structures in a “near-native” state. However, cryo-TEM provides limited chemical information on thin samples ($\lesssim$ 750 nm) within a narrow field of view (100s nm). On the other hand, SHXM is effective at characterizing, at the micron scale, millimeter-scale areas of poorly concentrated samples (10s of ppm). Ultimately correlating cryo-TEM with cryo-SHXM data sets of the same sample region allows the linking of sub-nm-scale structural information to crucial chemical speciation data. Here we use this approach to investigate the distribution and speciation of selenium in biofilms from an unconfined aquifer adjacent to the Colorado River, near Rifle, CO. The shallow groundwater has residual metal contamination (U, V, As, and Se) at tens of μM levels due to past ore-milling activities. These levels exceed U.S. Environmental Protection Agency (EPA) drinking water standards (100 nM for Se). To date, the potential for acetate amendments into the subsurface to stimulate uranium bioreduction has been extensively studied,(14-17) whereas microbiological and geochemical processes controlling selenium mobility, and thus toxicity at the site, and other similar sites are poorly understood.

Se occurs predominantly in four oxidation states (VI, IV, 0, and −II). Se oxyanions, Se(VI) selenate (SeO_4^{2-}) and Se(IV) selenite (SeO_3^{2-}), are toxic at ppm concentrations and known to bioaccumulate in the food chain, causing significant ecological damage.(18) The biogeochemical cycle of Se in nature is not well-defined(19) but is predominantly governed by microorganisms.(20)An important part of this cycle is the dissimilatory(21) reduction of Se oxyanions (DSeR) by anaerobes.(22) These microorganisms couple the oxidation of organic matter (or H_2) to the reduction of Se oxyanions, forming either relatively insoluble nontoxic Se^0 or reactive and toxic selenide Se(−II). Dissimilatory selenate reduction to Se^0 is a major sink for Se oxyanions in anoxic environments.(22, 23) Although phylogenetically diverse selenite-reducing bacteria have been well-characterized, relatively little is known about selenate-reducing bacteria. Moreover, the stability, reactivity, and bioavailability of Se^0 colloids are still not well understood and likely depend strongly on the size, morphology, and allotropic form of Se. A handful of studies have reported microbial reduction of Se oxyanions to Se^0, mostly as red amorphous(24-28) (primarily chain structures) and red crystalline

monoclinic(29) (Se_8 rings). However, few provide direct evidence of the structure of the Se allotropes produced, especially from field-preserved samples.

Previously at the Rifle site, microbial reduction of Se oxyanions was detected during a biostimulation experiment,(30) but many questions remained about the form(s) and distribution of the products. Here we developed a cryostage that allows the transfer of cryogenically preserved Se-rich biofilms between a TEM and a SHXM, enabling the acquisition of essentially artifact-free ultrastructural biological and chemical information from the same sample region. We used this approach to examine in detail the spatial distribution and chemical speciation of selenium in samples obtained through field experimentation at the Rifle site and cultivation.

Materials and Methods

Additional materials and methods can be found in the Supporting Information.

Biofilm Samples from the Rifle Site

The samples were collected during the "Super 8" uranium biostimulation field experiment(17) (August–September 2010) at the Rifle Integrated Field Research Challenge site adjacent to the Colorado River (Western Colorado, United States). The site is located on a relatively low-lying alluvial terrace created by a floodplain meander of the Colorado River and is described extensively elsewhere.(14, 16) The shallow, unconfined aquifer consists of alluvial sands, silts, and gravels; details on the geochemistry and mineralogy can be found in prior studies.(15, 16) As previously described,(17) the groundwater was amended with sodium acetate and injected into the subsurface at various depths. Acetate (CH_3COO^-) served as a carbon source and electron donor over the course of the 25 day amendment period. Biofilm samples were collected at well CG02 (4 m depth, 5 mM acetate), close to the down-gradient reference well CD01, 16 days after injection of acetate to the anoxic aquifer. For all analyses except confocal laser scanning microscopy, samples were collected by scraping the biofilm off the injection tubing (high density polyethylene) used to circulate the acetate-amended groundwater (pH ~7.2). The biofilms were uniformly distributed across the tubing and had minimal O_2 (from diffusion across the tubing wall) and low nitrate levels (~10 μM average). Samples were flash-frozen directly in the field to preserve their physical and chemical integrity using a portable cryoplunger(31) and procedures described in the Supporting Information.

Enrichment Cultures

For enrichment cultivation, we sampled pieces of the tubing used to deliver acetate to the subsurface in which a biofilm had grown onto the inner surface and preserved these pieces at −80

°C. Some pieces of biofilm were used for PCR amplification of 16S rRNA gene sequencing (see details in Supporting Information). Other pieces of biofilm were thawed and added anaerobically to fresh medium in a glovebox. Cultures were established either in 10 mL carbonate-buffered freshwater medium (sulfate and nitrate free) or in groundwater artificial medium (GWA, contains sulfate) and inoculated with sodium selenate or sodium selenite (5 mM, Sigma-Aldrich) and sodium acetate or sodium L-lactate (10 mM, Sigma-Aldrich). Details regarding the growth media can be found in the Table S1. Cultures were sparged with N_2/CO_2 (80:20) to remove dissolved oxygen and sealed with butyl rubber stoppers and aluminum crimp seals, as previously described.(32) All cultures were incubated at room temperature in the dark. Only cultures grown anaerobically using acetate as the carbon source and electron donor and selenate as the sole electron acceptor were further analyzed. Red precipitates were observed after 5 days, suggesting selenate reduction to Se^0. Samples were flash-frozen in the lab at various time points then stored in LN_2 until analyses.

2D Cryo-TEM

Cryo-TEM images were acquired with a JEOL-3100-FFC electron microscope (JEOL Ltd., Akishima, Tokyo, Japan) equipped with a FEG electron source operating at 300 kV, an Omega energy filter (JEOL), an LN_2-cooled sample-transfer stage (80 K), and a Gatan 795 4K × 4K CCD camera (Gatan Inc., Pleasanton, CA, USA) mounted at the exit of an electron decelerator held at a voltage of 200 to 250 kV. Survey of the grids and selection of suitable targets were performed in low-dose defocused diffraction mode. Images were recorded at different magnifications, with a pixel size of 0.56 and 0.701 nm at the specimen. Several images were recorded with a 2K × 2K CCD camera instead, with a pixel size of 0.69, 0.92, and 1.2 nm at the specimen. Underfocus values ranged from 12 ± 0.5 µm to 15 ± 0.5 µm, and energy filter widths were typically around 30 eV. Over 100 images of field samples and 70 images of culture samples were recorded to evaluate the morphology and size of cells and colloidal particles.

X-Ray Microprobe

Microfocused X-ray fluorescence (µXRF) mapping, X-ray diffraction (µXRD), and Se K-edge X-ray absorption spectroscopy data were collected at the Advanced Light Source (ALS) bending-magnet beamline 10.3.2 (2.4–17 keV) with the storage ring operating at 500 mA and 1.9 GeV.(33) All data were recorded at 95 K using a cryostage described below. Maps and µXRF spectra were collected at 13 keV with a beam spot size ranging from 2 × 2 µm to 5 × 5 µm, and counting times up to 200 ms per pixel. Fluorescence emission counts were recorded using a seven-element Ge solid-state detector (Canberra) and XIA electronics. Se K-edge µXANES spectra were recorded in fluorescence mode by continuously scanning the Si (111) monochromator (Quick XAS mode) from 160 eV below

up to 407 eV above the edge (12500–13067 eV, i.e., up to $k = 10$ Å^{-1}). EXAFS spectra were recorded up to 740 eV above the edge (12500–13400 eV, i.e., up to $k \approx 13.7$ Å^{-1}). Spectra were calibrated using the white line of a red amorphous Se standard set at 12660 eV. All data were processed using LabVIEW custom software and standard procedures described elsewhere.(34) To rapidly survey the valence state of selenium in the samples, we generated valence-state scatter plots from XANES data using a spectral database of Se compounds (see Table S2). Furthermore, least-squares linear combination fitting of the XANES spectra was performed as previously described.(35) Micro-EXAFS spectra of cultures were reduced with $k^2\chi(k)$ weighting, out to $k = 12$ Å^{-1}, and analyzed via shell-by-shell fitting using the FEFF6l code and the Artemis software.(36, 37) Only the first shell was fitted because other shells were not visible enough for accurate analysis. The structure of trigonal Se^0 as described by Keller and co-workers(38) was used to create FEFF6l input files from which Se–Se paths out to 3.5 Å could be extracted and fit to the experimental *t*-Se EXAFS spectrum at 95 K. The fits of the culture data were performed in q-space (2–12 Å) using a Kaiser-Bessel window (1.4–2.5 Å). Details on µXRD analyses can be found in the Supporting Information.

Correlative Cryogenic SHXM and TEM

A custom X-ray microprobe cryo-stage (−190 to +150 °C, ± 0.1 °C precision) was designed and built in collaboration with Instec Inc., to fit the geometry of the beamline and allow the cryotransfer of flash-frozen samples (Figures 1 and the Supporting Information). The apparatus allows cryo-XRF and cryo-XAS measurements to be performed in fluorescence or transmission modes. XRD measurements in transmission can be used to check for ice contamination and quality of the transfer. The apparatus consists of four parts: a stage (CLM77K), a sample loading frame (SLF) that can accommodate two round sample grid boxes, a grid-holder tongue (GHT), and a temperature controller (mk1000). Prior to any cold experiment, the CLM77K stage is heated to +110 °C for 5 min then purged with dry N_2 gas to remove any moisture trapped. The CLM77K is cooled to −190 °C (83 K) using a pressurized LN_2 tank. During cooling, the sample chamber and all windows are purged with dry N_2 gas to prevent water-vapor condensation and frost. The SLF, placed in a LN_2 bath in a Styrofoam container, is used to support the GHT during sample loading and unloading. Using the SLF, a single cryo-TEM grid (or Si_3N_4 window), mounted in a JEOL 3100 TEM cartridge, can be loaded onto the GHT for correlative analyses. Alternatively, another GHT designed to accommodate up to three TEM grids (or windows) can also be used. In either configuration, the spring-loaded GHT cover snaps closed over the cryo-TEM grids, keeping them thermally insulated. Once the CLM77K is cooled and stable at −190 ± 0.1 °C, the GHT containing the cryosamples is then quickly inserted

and locked into the CLM77K, where the sample temperature reaches 95 K. Thermocouples located in the GHT and CLM77K and connected to the mk1000 are used to continuously monitor (every second) the temperature of the sample and the stage, respectively. Once the cryo-microprobe measurements (~12 h maximum duration) are complete, the GHT with samples is cryotransferred back to the SLF in an LN_2 bath and samples are subsequently stored in LN_2.

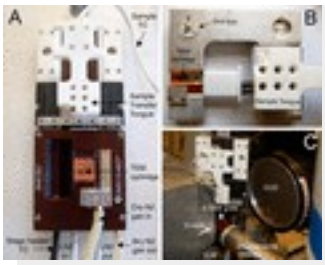

Figure 1. SHXM cryostage allowing correlative cryogenic TEM and microprobe measurements. (A) CLM77K stage with the JEOL 3100 TEM cartridge sample-transfer tongue inserted. (B) View of the cartridge-grid-holder tongue installed on the mounting frame. (C) View of the stage at beamline 10.3.2 with the sample-transfer tongue inserted. The sample is oriented at 45° to the incident beam, and micro-XRD is performed in transmission mode.

Results and Discussion

Geochemistry

Biofilm samples (referred as “biofilm CG02”) were collected 16 days after the start of acetate amendment in the subsurface, during the Fe(III) reduction period.(39) Acetate injection into the aquifer resulted in a rapid decrease of soluble Se; the minimum concentration was reached after 7 days (Figure S2). The concentration of dissolved Se (Se oxyanions) just prior to acetate injection on day 1 was 0.81 μM, versus 0.03 μM on day 15 (the closest time point to sample collection), suggesting that ~96% of dissolved Se was converted into a solid phase. Soluble Se concentration remained well below the U.S. EPA limit for Se in drinking water (0.1 μM) past the biostimulation experiment. Sulfate concentrations remained stable, indicating minimal sulfate reduction and sulfide production during the sampling period. These trends are consistent with prior acetate biostimulation experiments(16) on unamended portions of the Rifle aquifer as was the case here.

Microbial Community Composition

Phylogenetic analyses of the 16S rRNA gene sequences recovered from biofilm CG02 show an abundance of organisms from the Betaproteobacteria class (72% of the community

sequences, Figures S3 and S4). These bacteria are often found to be dominant in freshwaters and are inferred to play an important role in the nitrogen cycle, including nitrate respiration. Comamonadaceae is the most abundant family (Figure S3C), and uncultivated members of the *Simplicispira* genus were the most abundant identified organisms (Figures S3D and S4B). It is well-known from prior studies at this site that acetate enriches for members of the Comamonadaceae family, specifically the *Simplicispira*(40) genus. In fact, this result was shown previously in well CD01, the same groundwater reference well used in the current study.(41) The facultative anaerobe *Simplicispira*strain BDI(42) (motile, weakly curved rod), a nitrate and vanadate reducer, was isolated from this site. We tested this isolate for selenate or selenite reduction to Se^0. The organism was cultivated both in nitrate-free and nitrate-amended (2 mM) bicarbonate freshwater medium inoculated with acetate (5 and 10 mM) and selenate (5 mM) or selenite (1, 2, and 5 mM). No red (or gray, black, or brown) Se^0 precipitates were formed, indicating that strain BDI does not carry out this transformation in solutions containing mM concentrations of these Se oxyanions. A large number of uncultivated members of the Comamonadaceae family were detected, some of which could contribute to the reduction of Se oxyanions. However, we could not test this hypothesis because to date, only the BDI strain has been isolated from this site. Some members of the Comamonadaceae family, such as *Comamonas sp.*, are known selenite reducers.(43) The identified genus from this family, *Hydrogenophaga sp.* (H_2-oxidizer), are rod-shaped, autotrophic denitrifiers(44) that have been correlated with nitrate and selenate fluxes.(45) These organisms likely contribute to selenate reduction because some strains have been reported to reduce selenate and selenite to dimethyl selenide (DMSe) and dimethyl diselenide (DMDSe).(46)

The second-most-abundant family detected was Rhodocyclaceae (Figures S3C and S4C), which contains many denitrifying bacteria. Among identified genera from this family, rod-shaped *Zoogloea sp.* (9%) contains strains capable of denitrification(47) and of selenite reduction to elemental Se. (48) *Zoogloea sp.* have also been previously detected in Se-rich biofilms from Rifle. (30) *Ferribacterium sp.*(49) and *Dechloromonas* RCB form a monophyletic group (Figure S4C) representing 5% of the bacterial community. *Dechloromonas sp.* are well-known perchlorate and nitrate-reducing bacteria(50) commonly found or used to enhance selenate reduction in bioreactors. (51, 52) *Hydrogenophaga sp.*, *Zoogloea sp.* and *Dechloromonas sp.* have been previously detected in Se-rich biofilms(30) at Rifle and have been often detected at this site over the years.(30, 53-57) Finally, bacteria from the Chloroflexi and the Bacteroidetes phyla could also contribute to selenate reduction because a variety of selenate reductases have been identified in the genomes of Anaerolineaceae and Bacteroidetes(58) obtained from the Rifle site (http://ggkbase.berkeley.edu/). .

Organisms from unidentified genera and uncultivated *Simplicispira* members account for nearly three-quarters of the bacterial community. Their potential role in Se oxyanions reduction is unknown and warrants further investigation. These results suggest uncultivated members of the Comamonadaceae family may play an important role in Se oxyanions reduction at this location.

Ultrastructure and Carbon Speciation of the Field and Culture Samples

The 3D confocal microscopy of biofilm CG02 revealed a 2 to 12 µm thick biofilm with several haystacks of self-organized cells (Movie S1). On the surface of the haystack, the cells range in size from 0.75 to 2.7 µm (Movie S2). Within the core and bottom of the stack, cells are similar in length but with an oval shape. In both the field and the culture samples, cells exhibited a Gram-negative cell wall with an inner membrane, an outer membrane, and a peptidoglycan layer within a periplasmic space (Figures 2 and S5). Cells were weakly curved rods, rod-, oval- or round-shaped, with the latter only observed in biofilm CG02. Few cells exhibited an S-layer; many had visible polar flagella or pili. Most bacteria from biofilm CG02 had pili (Figure S5). Most cells contained cytoplasmic granules. STXM-derived C K-edge XANES spectra of granules (Figure S6) exhibits a major peak at 288.4 eV, attributed to carboxyls or esters,(59, 60) likely associated with polyhydroxyalkanoates (polyesters), carbon, and electron and energy storage polymers commonly produced by bacteria under limited nutrients. Carbon storage granules have been widely reported in organisms we detected by 16S rRNA, such as *Simplicispira sp.*,(40) *Dechloromonas sp.*, (61)*Hydrogenophaga sp.*(62) *and Zoogloea sp.*.(47, 63) Further, a prior study(64) on members of the Comamonadaceae family showed that a N-poor medium tends to stimulate the production of polyhydroxyalkanoates, whereas a C-poor environment leads to the production of polyphosphates. Carbon K-edge STXM data on field and culture samples (Figures S6 and S7) showed abundant Se-rich aggregates associated with a thick protein-rich biofilm matrix containing extracellular polymeric substances (EPS) rich in acidic polysaccharides, with a peak at 288.6 eV (π*(C=O) transition of carboxyl group in acidic polysaccharides) and in carbonates, with a signature π*(C=O) peak at ~290.3 eV. In the cultures, Se^0 CNPs located near cell surfaces were coated with a protein-rich organic layer (Figure S7).

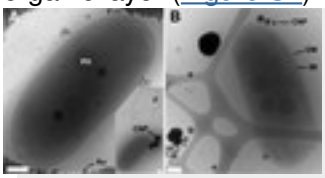

Figure 2. Cryo-TEM images of anaerobes, colloidal nanoparticles, and aggregates from (A) biofilm CG02 and (B) selenate-reducing enrichment culture (19 days old) grown in bicarbonate medium. IM indicates inner membrane, OM indicates outer membrane, F indicates flagellum, PH indicates polyhydroxyalkanoates, CNP

indicates colloidal nanoparticles, and Au indicates gold fiducial particles on a carbon-coated lacey Formvar film. Scale bars are 200 nm.

Selenium Distribution and Speciation in the Field and Culture Samples

In both the field and the culture samples, the vast majority of colloidal nanoparticles (CNPs) were found as extracellular aggregates or as a few electron dense particles on cell surfaces. SEM imaging and energy dispersive spectroscopy of these particles (Figure S8) showed Se, with traces of Ca (and Si) from the background medium. The biofilm CG02 particles were about 160 nm ±70 nm in diameter, while the particles in the culture grown in bicarbonate medium were a bit smaller at about 130 ± 70 nm (Figure S9). Only a few Se CNPs were found on each individual cell surface as seen from TEM and STXM data. Se $L_{2,3}$ edges XANES spectra of CNPs compared to those of model compounds are shown in Figure S10. The spectra of Se standards are consistent with prior reports, (65, 66) and spectra of CNPs from field and culture samples closely match that of red amorphous Se^0. However, the allotropic form of Se cannot be accurately determined at these absorption edges, and thus, further analysis of these spectra was not pursued.

By contrast, most Se compounds can easily be classified by K-edge XANES due to a clear shift (2–3 eV) of the edge position ("white line") depending on Se oxidation state (Figure 3). This can be explained by dipole selection rules where 1s core electrons are excited into the unoccupied 4p electronic states, and where the edge position shifts toward higher energy as the oxidation state increases. Standard spectra are consistent with prior studies.(67-70) Twenty nine Se-rich regions were investigated by µXANES on biofilm CG02, 18 on cultures grown in bicarbonate, and 23 on cultures grown in GWA medium to get enough statistics. Cultures were analyzed up to 60 days after the addition of selenate and acetate to the medium to determine the end products. Typical Se K-edge XANES of the CNPs from biofilm CG02 and cultures grown in bicarbonate medium are displayed in Figure 3 and most closely resemble that of red amorphous Se. Se valence plots and least-squares linear combination fitting (LSQF) of the XANES spectra (see the Materials and Methods section and Supporting Information) indicate that red amorphous Se^0 is the major end product in all samples (Figure 4 and Table S3). Attempts at fitting the data with other Se^0compounds, such as red monoclinic-α Se, black amorphous Se, and gray hexagonal Se, did not yield good fits. These results were further confirmed by µXRD (Figure S11) on field and culture samples that showed no evidence for crystalline Se (either hexagonal or monoclinic). There is an accumulation of selenite during selenate reduction in the culture samples that is not observed in the field data, as evidenced in both the valence plot (Figure 4) and fitting results (Table S3).

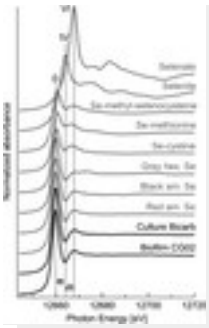

Figure 3. Se K-edge µXANES spectra of biofilm CG02 and of a 19 day old culture grown in bicarbonate medium, compared with a subset of standards (see Table S2 for the complete list). Normalized XANES values at 12664.25 (IV, dashed line) and 12667.8 eV (VI, dashed line) were used to generate the Se valence-state plot displayed in Figure 4 (see the Supporting Information).

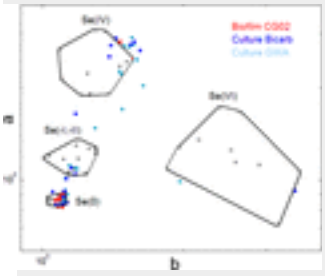

Figure 4. Se valence-state scatter plot. The standards are shown in open black squares, the biofilm CG02 in red (29 spots), and the enrichment cultures grown in bicarbonate medium in dark blue (18 spots) or in groundwater artificial medium in light blue (23 spots). The Se(−II, −I) group includes organic Se compounds. See the Materials and Methods section and the Supporting Information for further details. Results of the least-squares linear combination fitting of all sample µXANES spectra are summarized in Table S3. Both analyses indicate that Se^0 is the main product in field-derived and culture samples.

Correlated cryogenic SHXM and TEM analyses of a 19 day old culture in bicarbonate medium are shown in Figure 5 and S11. A cluster of bacteria is found associated with ∼100 ± 60 nm diameter Se^0 CNPs and traces of Se(IV). Organo-selenium and inorganic selenides were not detected in this region, suggesting that reduction proceeds in a two-step reaction from Se(VI) to Se(IV) to Se(0). Compared to the results of a prior study on Se-rich biofilm,(30) correlated cryogenic SHXM and TEM allows the identification of the forms of selenium present on intact organisms and resolution of their ultrastructure and associated minerals. Considering the low X-ray dose applied to the frozen samples (see the Supporting Information), photoreduction is an unlikely explanation for the formation of these compounds. The corresponding µXRD spectrum (Figure S11B) does not show a match to crystalline Se^0 (either hexagonal or monoclinic). Furthermore, we compared the EXAFS spectra of Se^0 CNPs from biofilm CG02 and bicarbonate cultures (Figure 6 and Table S4) with those of the

crystal structure of hexagonal Se^0, as determined by Keller et al.(38) The first shell (Se–Se bond) lies at 2.355 ± 0.003 Å for the biofilm CG02 and at 2.339 ± 0.003 Å for the bicarbonate culture, respectively. These interatomic distances are shorter than the bond length in hexagonal Se (2.374 Å) and are consistent with previous reports for amorphous Se.(71, 72) Only the first shell could be fitted by a shell-by-shell method; the second shell was not sufficiently visible to fit due to lack of structural order, and thus the Se–Se–Se bond angle could not be determined. The coordination numbers (N) and sigma square (σ^2) values of the samples are very similar. The biofilm CG02 exhibits the longest bond length among the two samples, reflecting a less disordered structure.

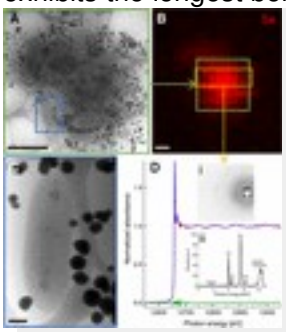

Figure 5. Correlative cryogenic spectromicroscopy on a 19 day old culture grown in bicarbonate medium. (A) Low-dose cryo-TEM image (3.5 nm pixels, 7.2 × 7.2 μm^2) of a cluster of bacteria and the associated Se CNP aggregates. (B) Cryo-μXRF Se distribution map at 13 keV (2 μm beam, 1 μm pixels). The green-box area represents the entire TEM region. C) Low-dose cryo-TEM image at higher magnification of the blue box area of panel A. (D) Cryogenic Se K-edge μXANES (in red) collected in the orange-box area of panel B. Best fit (in blue) is obtained using 87% red amorphous Se and 13% sodium selenite standards. Residual is plotted in green (normalized sum-square is 1.25×10^{-4}). Insets (i) and (ii): Cryo-μXRD pattern and -μXRF spectrum, respectively, collected at 17 keV in the orange-box area. XRD showed no evidence for crystalline Se^0 (see Figure S11). Red amorphous Se^0 aggregates (~100 ± 60 nm) is the main product of selenate reduction in this region of the sample, with a minor presence of Se(IV), suggesting a two-step reduction process. Scale bars are 2 μm (A,B) and 200 nm (C).

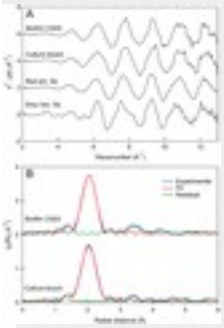

Figure 6. Cryo-μEXAFS of biofilm CG02 and of a 19 day old selenate-reducing enrichment culture grown in bicarbonate medium (A) in k-space, compared to red amorphous Se^0 and hexagonal gray Se^0 (Se foil) standards. (B) Shell-by-shell fitting analysis of the first shell (see Table S4) with Se–Se interatomic distance

at 2.355 ± 0.003 Å for the biofilm CG02 and 2.339 ± 0.003 Å for the culture. Experimental spectra are shown in blue, and the fits (performed in q-space) in red and the residuals in green.

Although a vast majority of the data indicated red amorphous Se^0, a few regions analyzed outside thick biofilm regions in the 19 day old culture show crystallization, as evidenced by diffraction contrast and the presence of planar defects, likely twin planes (Figure S12). It is interesting that crystallization occurred over just 19 days at 25 °C, given that the transformation of bulk red amorphous Se to gray trigonal Se should occur at appreciable rates only above ∼50 °C. (73)Nonetheless, in both the cultures and the field samples, red amorphous Se was stable for months.

Dissimilatory and Assimilatory Selenate Reducers

Cryospectromicroscopy and 16S rRNA gene sequence analysis of field and culture samples suggest the presence of DSeR organisms. In that process, selenate used as the sole terminal electron acceptor is sequentially reduced to selenite and Se^0 and further to selenide. Our cultivation conditions involved high selenate concentration and resulted in significant production of red amorphous Se (∼30% of the volume). Dissimilatory reduction of selenate and selenite by anaerobic bacteria generally produces abundant extracellular Se^0 particles,(29) consistent with our observations. Selenite is a known intermediate in the microbial dissimilatory reduction of selenate, being produced and reduced concomitantly. By contrast, the assimilatory microbial reduction of selenate does not produce selenite(20) but leads to the formation of organoselenium and selenides, both being found as minor components in our samples. Selenite can be dissimilatory reduced to Se^0 and further to selenide (e.g., H_2Se) or it can be reduced via assimilation to organoselenium (e.g., SeMet) and volatile selenides (e.g., DMSe)(74)

The presence of organic Se in our samples could be attributed to either cell lysis, selenate-tolerant bacteria, or (potentially) selenite-to-selenide reducing bacteria. Selenate reduction is mediated by either a soluble periplasmic selenate reductase (SerABC) or a nitrate reductase or via a dissimilatory sulfate-reducing pathway. A wide variety of selenate reductases have been identified in the genomes of bacteria from the Rifle site (http://ggkbase.berkeley.edu/). Selenite is usually imported into the cytoplasm, where it is reduced to Se^0 via a membrane-associated reductase followed by the rapid expulsion of Se particles via a membrane efflux pump.(75) Selenite is reduced by reacting with proteins in a “Painter-type” reaction, suggested as a general microbial detoxification reaction to Se oxyanions.(76)

When sulfate-containing media (GWA) is used, some sulfate-reducing anaerobes could also be capable of reducing μM amounts of selenate, although they generally do not couple this reduction to

growth.(28, 77) Moreover, the ability of sulfate respirers to reduce selenate (or selenite) is greatly constrained by the availability of sulfate. Se oxyanions are thermodynamically predicted to be reduced prior to sulfate(22) according to their respective redox potentials (+0.44 V for SeO_4^{2-} and SeO_3^{2-}, + 0.21 V for SeO_3^{2-} and Se^0, −0.22 V for SO_4^{2-} and H_2S, and −0.52 V for SO_4^{2-} and SO_3^{2-}). At the shallow depth (4 m) where biofilms were collected, the sulfate concentration (8 mM, Figure S2) is at a level that usually precludes selenate reduction by sulfate reducers.(21, 77) By contrast, DSeR microorganisms can reduce mM amounts of selenate to Se^0, consistent with our observations. In part due to similar potentials for the SeO_4^{2-} and SeO_3^{2-} (+0.44 V) and NO_3^- and NO_2^- (+0.42 V) redox couples, microbial reduction of nitrate and selenate often occur close together,(78, 79) consistent with the presence of denitrifying bacteria we find by 16S rRNA gene sequencing analyses.

Accumulation of Selenite in Cultures

The accumulation of selenite observed during growth on selenate, regardless of the medium used, could occur because the microbial community reduces selenate faster than selenite. Alternatively, Se oxidizers may reoxidize Se^0 to selenite. The first hypothesis is the most likely because reduction of selenite to red Se^0 by the cultures was minimal and occurred very slowly (over weeks). The oxidation of Se^0 by Se-oxidizers cannot be ruled out, considering the large pool of unidentified organisms; however, that process is generally very slow.(80) More importantly in our cultures, cells are under different geochemical conditions than in the field and are subjected to concentrations of Se oxyanions orders of magnitude higher (5 mM versus ∼1 μM), selectively enriching for few members of the community.

Association of Red Amorphous Se CNPs with Proteins

Our results show that Se^0 CNPs are strongly associated with proteins in the biofilm.(81, 82)Particles may be surface-stabilized from dissolution or phase transformation when embedded in the protein-rich biofilm matrix, as suggested by prior research on biogenic and synthetic Se^0nanoparticles in the presence of proteins.(83, 84) Previous studies have suggested the presence of surface-associated proteins on Se^0 produced by selenite reducers.(85) More generally, prior studies have shown that biogenic (and synthetic) selenium nanoparticles can be associated with a plenitude of high-affinity proteins.(83, 86) Proteins, peptides, and amino acids could be released after cell death(87) and scavenged by hydrophobic elemental selenium surfaces. Alternatively, bacteria may also excrete Se-binding proteins.(24) Finally, Se^0 particles found outside cells could have been released through cell lysis,(28) as we have observed in old culture samples. Any of these processes would lead to extracellular aggregation of Se^0 nanoparticles, preventing entombment of cells. The aggregation of Se particles likely affects selenium mobility and transport,(88) as evidenced by prior work showing

that aggregation induced by extracellular metal-binding polypeptides and proteins plays an important role in constraining the dispersion of nanoparticles in the environment.(89)

Many anthropogenic activities (e.g., agriculture, petroleum refining, mining, glass, and pigment manufacturing) generate Se- contaminated wastewaters. Existing treatment technologies, based on chemical coprecipitation or adsorption, are rather inefficient (especially for selenate) and too expensive for practical industrial use. Bioremediation represents an attractive alternative approach but strongly relies on determining accurately the chemical speciation and distribution of the bioreduction products to be directly applicable to a diversity of anaerobic soil and groundwater environments contaminated with selenium.

The community of Se oxyanions reducers detected here includes several genera previously detected in Se-rich biofilms collected under similar conditions at the Rifle site.(30) However, the distribution patterns and allotropic form of selenium found here are clearly distinct. The prior study suggested the presence of cells encrusted with red monoclinic Se^0, but using our novel correlative cryogenic spectro-microscopy apparatus, we demonstrate that the main product is extracellular red amorphous Se^0 captured in a protein-rich biofilm matrix and that only a few particles are associated with each cell surface. Both the newly identified protein coating and extensive particle aggregation are expected to reduce reoxidation rates, thereby minimizing the rapid rerelease of aqueous Se to the environment.

Supporting Information

The Supporting Information is available free of charge on the ACS Publications website at DOI: 10.1021/acs.est.5b01409.

- Movie showing 3D confocal microscopy of biofilm CG02 revealing a 2 to 12 µm thick biofilm with 262 several haystacks of self-organized cells (AVI)
- Movie showing haystack-surface cells (AVI)
- Materials and methods for groundwater geochemical measurements, cryoplunging of samples for synchotron and TEM analyses, selenium valance-state scatter plots, micro-X-ray diffraction, confocal laser-scanning microscopy, 16S ribosomal RNA gene sequencing and phylogenetic analysis, scanning transmission x-ray microscopy, and SEM/EDS. Supplementary

text on X-ray radiation dose rate estimates. Figures showing the experimental setup and temperature profiles of the cryostage, concentrations of soluble materials as a function of time, relative abundances within the Rifle CG02 biofilm microbial community, maximum-likelihood 16S rRNA gene and neighbor-joining phylogenetic trees, cryogenic transmission electron micrographs of organisms present in the biofilm, STXM C K-edge data on biofilm and measurements on culture grown in GWA media, scanning electron microscopy and energy-dispersive spectroscopy of Se^0 SNPs in biofilm and biocarbonate culture, the size distribution of SNPs in biofilm and bicarbonate cultures, µXRD profiles of biofilm and bicarbonate culture, and CLSM of field-derived biofilms. Tables showing the content of growth media employed, a list of the selenium standard compounds used in valence plot and LSQ linear-combination fitting analyses, summary of results of the LSQ linear combination fitting of XANES spectra on biofilms and enrichment cultures, and EXAFS fitting parameters (PDF)

- SeK standards (ZIP)

- **Microsoft Video (AVI)**
  - es5b01409_si_001.avi (17.13 MB)
  - es5b01409_si_002.avi (1.55 MB)

- **PDF**
  - es5b01409_si_003.pdf (2.24 MB)
- **Zip**
  - es5b01409_si_004.zip (58.18 kB)

Correlative Cryogenic Spectromicroscopy to Investigate Selenium Bioreduction Products

Showing 1/4: es5b01409_si_004.zip

SeK_standards

AmorphousSeshot_CRYO.e

AmorSeshot_RT.e

BaSelenate_CRYO.e

Black99Se_RT.e

Caselenate_RT.e

Caselenite_CRYO.e

CuIIselenite_CRYO.e

cupric_selenate_RT.e

GreySe_CRYO.e

GreySe_RT.e

KSelenate_CRYO.e

magnesiumselenate_CRYO.e

neodymiumselenate_CRYO.e

RedSe_CRYO.e

RedSe_RT.e

Se_tetrachloride_RT.e

Sedioxide_CRYO.e

Sefoil_CRYO.e

Sefoil_RT.e

Seleno_DL_cystine_CRYO.e

Seleno_DL_methionine_CRYO.e

SeMethylselenocysteine_CRYO.e

Sodium Selenate_CRYO.e

Sodium Selenite_CRYO.e

SynthRedSe_193nm_RT.e

SyntRedSe_193nm_CRYO.e

Znselenate_CRYO.e

Znselenite_CRYO.e

⊥Author Present Address

B.L.: Department of Biotechnology, Norwegian University of Science and Technology, Trondheim 7491, Norway.

#Author Present Address

S.W.M.: Division of Geological and Planetary Sciences, California Institute of Technology, Pasadena, CA 91125.

The authors declare no competing financial interest.

Acknowledgment

This material is partially based on work supported through the Lawrence Berkeley National Laboratory's Sustainable Systems Scientific Focus Area. The U.S. Department of Energy Office of Science and the Office of Biological and Environmental Research funded the work under contracts DE-SC0004733 and DE-AC02-05CH11231. Part of the equipment was funded by the LBL EFRC Center for Nanoscale Control of Geologic CO_2. We thank Paul Baker at Instec Inc. for his help with the microprobe cryostage, Sue Spaulding for lab support, Tolek Tylizscack for support at ALS beamline 11.0.2, and Mary Gilles and Steve Kelly for sharing their ESEM. We are grateful to D. Strawn, A. Ryser, E.A.H. Pilon-Smits, and J.L. Freeman for sharing their selenium standard spectra. The Advanced Light Source is supported by the Office of Basic Energy Sciences, Office of Science, U.S. Department of Energy contract no. DE-AC02-05CH11231.

Reference QuickView

References

This article references 89 other publications.

1. 1.

   Dohnalkova, A. C.; Marshall, M. J.; Arey, B. W.; Williams, K. H.; Buck, E. C.; Fredrickson, J. K. Imaging Hydrated Microbial Extracellular Polymers: Comparative Analysis by Electron Microscopy *Appl. Environ. Microbiol.* **2011**, 77 (4) 1254– 1262 DOI: 10.1128/AEM.02001-10

   [Crossref], [PubMed], [CAS]

2. 2.

   Manceau, A.; M, A. M.; Tamura, N. *Appl. Synchotron Radiat.* **2002**, 49 (1) 341

3. 3.

Howells, M. R.; Hitchcock, A. P.; Jacobsen, C. J. Introduction: Special issue on radiation damage *J. Electron Spectrosc. Relat. Phenom.* **2009**, 170 (1–3) 1– 3 DOI: 10.1016/j.elspec.2009.01.004

[Crossref], [CAS]

4. 4.

Fayard, B.; Salomé, M.; Takemoto, K.; Kihara, H.; Susini, J. Some practical considerations about the effects of radiation damage on hydrated cells imaged by X-ray fluorescence microscopy *J. Electron Spectrosc. Relat. Phenom.* **2009**, 170 (1–3) 19– 24 DOI: 10.1016/j.elspec.2008.11.003

[Crossref], [CAS]

5. 5.

Cody, G. D.; Brandes, J.; Jacobsen, C.; Wirick, S. Soft X-ray induced chemical modification of polysaccharides in vascular plant cell walls *J. Electron Spectrosc. Relat. Phenom.* **2009**, 170 (1–3) 57– 64DOI: 10.1016/j.elspec.2008.09.007

[Crossref], [CAS]

6. 6.

Holton, J. XANES measurements of the rate of radiation damage to selenomethionine side chains *J. Synchrotron Radiat.* **2007**, 14 (1) 51– 72 DOI: 10.1107/S0909049506048898

[Crossref], [PubMed], [CAS]

7. 7.

George, G. N.; Pickering, I. J.; Pushie, M. J.; Nienaber, K.; Hackett, M. J.; Ascone, I.; Hedman, B.;Hodgson, K. O.; Aitken, J. B.; Levina, A.; Glover, C.; Lay, P. A. X-ray-induced photo-chemistry and X-ray absorption spectroscopy of biological samples *J. Synchrotron Radiat.* **2012**, 19 (6) 875– 886 DOI: 10.1107/S090904951203943X

[Crossref], [PubMed], [CAS]

8. 8.

Huggins, F. E.; Sanei, H. Synchrotron-radiation-induced oxidation of selenite to selenate in coal-derived fly ash *J. Synchrotron Radiat.* **2011**, 18 (3) 530– 533 DOI: 10.1107/S0909049511002627

[Crossref], [PubMed], [CAS]

9. 9.

Lenz, M.; van Hullebusch, E. D.; Farges, F.; Nikitenko, S.; Corvini, P. F. X.; Lens, P. N. L. Combined Speciation Analysis by X-ray Absorption Near-Edge Structure Spectroscopy, Ion Chromatography, and Solid-Phase Microextraction Gas Chromatography–Mass Spectrometry

To Evaluate Biotreatment of Concentrated Selenium Wastewaters *Environ. Sci. Technol.* **2011**, 45 (3) 1067– 1073 DOI: 10.1021/es1022619

[ACS Full Text], [CAS]

10. 10.

Kolobov, A. V.; Oyanagi, H.; Tanaka, K.; Tanaka, K. Structural study of amorphous selenium by in situ EXAFS: Observation of photoinduced bond alternation *Phys. Rev. B: Condens. Matter Mater. Phys.* **1997**,55 (2) 726– 734 DOI: 10.1103/PhysRevB.55.726

[Crossref]

11. 11.

Milne, J. L. S.; Subramaniam, S. Cryo-electron tomography of bacteria: progress, challenges and future prospects *Nat. Rev. Microbiol.* **2009**, 7 (9) 666– 675 DOI: 10.1038/nrmicro2183

[Crossref], [PubMed], [CAS]

12. 12.

Comolli, L. R.; Banfield, J. F. Inter-species interconnections in acid mine drainage microbial communities*Front. Microbiol.* **2014**, 5, 367 DOI: 10.3389/fmicb.2014.00367

[Crossref], [PubMed], [CAS]

13. 13.

Comolli, L. R.; Downing, K. H. Dose tolerance at helium and nitrogen temperatures for whole cell electron tomography *J. Struct. Biol.* **2005**, 152 (3) 149– 156 DOI: 10.1016/j.jsb.2005.08.004

[Crossref], [PubMed], [CAS]

14. 14.

Anderson, R. T.; Vrionis, H. A.; Ortiz-Bernad, I.; Resch, C. T.; Long, P. E.; Dayvault, R.; Karp, K.;Marutzky, S.; Metzler, D. R.; Peacock, A.; White, D. C.; Lowe, M.; Lovley, D. R. Stimulating the In Situ Activity of Geobacter Species To Remove Uranium from the Groundwater of a Uranium-Contaminated Aquifer *Appl. Environ. Microbiol.* **2003**, 69 (10) 5884– 5891 DOI: 10.1128/AEM.69.10.5884-5891.2003

[Crossref], [PubMed], [CAS]

15. 15.

Campbell, K. M.; Kukkadapu, R. K.; Qafoku, N. P.; Peacock, A. D.; Lesher, E.; Williams, K. H.; Bargar, J. R.;Wilkins, M. J.; Figueroa, L.; Ranville, J.; Davis, J. A.; Long, P. E. Geochemical, mineralogical and microbiological characteristics of sediment from a naturally reduced zone in a uranium-contaminated aquifer*Appl. Geochem.* **2012**, 27 (8) 1499– 1511 DOI: 10.1016/j.apgeochem.2012.04.013

[Crossref], [CAS]

16. 16.

Williams, K. H.; Long, P. E.; Davis, J. A.; Wilkins, M. J.; N'Guessan, A. L.; Steefel, C. I.; Yang, L.;Newcomer, D.; Spane, F. A.; Kerkhof, L. J.; McGuinness, L.; Dayvault, R.; Lovley, D. R. Acetate Availability and its Influence on Sustainable Bioremediation of Uranium-Contaminated Groundwater *Geomicrobiol. J.***2011**, 28 (5–6) 519– 539 DOI: 10.1080/01490451.2010.520074

[Crossref], [CAS]

17. 17.

Bao, C.; Wu, H.; Li, L.; Newcomer, D.; Long, P. E.; Williams, K. H. Uranium Bioreduction Rates across Scales: Biogeochemical Hot Moments and Hot Spots during a Biostimulation Experiment at Rifle, Colorado*Environ. Sci. Technol.* **2014**, 48 (17) 10116– 10127 DOI: 10.1021/es501060d

[ACS Full Text], [CAS]

18. 18.

Santolo, O. H. M. a. G. M., Kesterson Reservoir-Past, Present, and Future: An Ecological Risk Assessment. In *Selenium in the Environment*; W.T. Frankenberger, J.; Benson, S.M., Eds.; Marcel Dekker: New York,**1994**; pp 69– 117.

19. 19.

Shrift, A. A Selenium Cycle in Nature? *Nature* **1964**, 201 (4926) 1304– 1305 DOI: 10.1038/2011304a0

[Crossref], [PubMed], [CAS]

20. 20.

W.T. Frankenberger, J.; Benson, S.M. *Selenium in the Environment*; Taylor & Francis: New York, **1994**.

[Crossref]

21. 21.

Lovley, D. R. Dissimilatory Metal Reduction *Annu. Rev. Microbiol.* **1993**, 47 (1) 263– 290 DOI: 10.1146/annurev.mi.47.100193.001403

[Crossref], [PubMed], [CAS]

22. 22.

Oremland, R. S.; Hollibaugh, J. T.; Maest, A. S.; Presser, T. S.; Miller, L. G.; Culbertson, C. W. Selenate Reduction to Elemental Selenium by Anaerobic Bacteria in Sediments and

Culture: Biogeochemical Significance of a Novel, Sulfate-Independent Respiration *Appl. Environ. Microbiol.* **1989**, 55 (9) 2333–2343

[PubMed], [CAS]

23. 23.

Steinberg, N. A.; Oremland, R. S. Dissimilatory Selenate Reduction Potentials in a Diversity of Sediment Types *Appl. Environ. Microbiol.* **1990**, 56 (11) 3550– 3557

[PubMed], [CAS]

24. 24.

Debieux, C. M.; Dridge, E. J.; Mueller, C. M.; Splatt, P.; Paszkiewicz, K.; Knight, I.; Florance, H.; Love, J.;Titball, R. W.; Lewis, R. J.; Richardson, D. J.; Butler, C. S. A bacterial process for selenium nanosphere assembly *Proc. Natl. Acad. Sci. U. S. A.* **2011**, 108 (33) 13480– 13485 DOI: 10.1073/pnas.1105959108

[Crossref], [PubMed], [CAS]

25. 25.

Hunter, W.; Manter, D. Reduction of Selenite to Elemental Red Selenium by Pseudomonas sp. Strain CA5*Curr. Microbiol.* **2009**, 58 (5) 493– 498 DOI: 10.1007/s00284-009-9358-2

[Crossref], [PubMed], [CAS]

26. 26.

Kessi, J.; Ramuz, M.; Wehrli, E.; Spycher, M.; Bachofen, R. Reduction of Selenite and Detoxification of Elemental Selenium by the Phototrophic Bacterium *Rhodospirillum rubrum Appl. Environ. Microbiol.* **1999**,65 (11) 4734– 4740

[PubMed], [CAS]

27. 27.

Tomei, F. A.; Barton, L. L.; Lemanski, C. L.; Zocco, T. G. Reduction of selenate and selenite to elemental selenium by Wolinella succinogenes *Can. J. Microbiol.* **1992**, 38 (12) 1328– 1333 DOI: 10.1139/m92-219

[Crossref], [CAS]

28. 28.

Tomei, F.; Barton, L.; Lemanski, C.; Zocco, T.; Fink, N.; Sillerud, L. Transformation of selenate and selenite to elemental selenium byDesulfovibrio desulfuricans *J. Ind. Microbiol.* **1995**, 14 (3–4) 329– 336 DOI: 10.1007/BF01569947

[Crossref], [CAS]

29. 29.

Oremland, R. S.; Herbel, M. J.; Blum, J. S.; Langley, S.; Beveridge, T. J.; Ajayan, P. M.; Sutto, T.; Ellis, A. V.;Curran, S. Structural and Spectral Features of Selenium Nanospheres Produced by Se-Respiring Bacteria*Appl. Environ. Microbiol.* **2004**, 70 (1) 52– 60 DOI: 10.1128/AEM.70.1.52-60.2004

[Crossref], [PubMed], [CAS]

30. 30.

Williams, K. H.; Wilkins, M. J.; N'Guessan, A. L.; Arey, B.; Dodova, E.; Dohnalkova, A.; Holmes, D.;Lovley, D. R.; Long, P. E. Field evidence of selenium bioreduction in a uranium-contaminated aquifer*Environ. Microbiol. Rep.* **2013**, 5 (3) 444– 452 DOI: 10.1111/1758-2229.12032

[Crossref], [PubMed], [CAS]

31. 31.

Comolli, L. R.; Duarte, R.; Baum, D.; Luef, B.; Downing, K. H.; Larson, D. M.; Csencsits, R.; Banfield, J. F. A portable cryo-plunger for on-site intact cryogenic microscopy sample preparation in natural environments*Microsc. Res. Tech.* **2012**, 75 (6) 829– 836 DOI: 10.1002/jemt.22001

[Crossref], [PubMed], [CAS]

32. 32.

Coates, J. D.; Phillips, E. J.; Lonergan, D. J.; Jenter, H.; Lovley, D. R. Isolation of Geobacter species from diverse sedimentary environments *Appl. Environ. Microbiol.* **1996**, 62 (5) 1531– 6

[PubMed], [CAS]

33. 33.

Marcus, M. A.; MacDowell, A. A.; Celestre, R.; Manceau, A.; Miller, T.; Padmore, H. A.; Sublett, R. E.Beamline 10.3.2 at ALS: a hard X-ray microprobe for environmental and materials sciences *J. Synchrotron Radiat.* **2004**, 11 (3) 239– 247 DOI: 10.1107/S0909049504005837

[Crossref], [PubMed], [CAS]

34. 34.

Kelly, S. D.; Hesterberg, D.; Ravel, B. Analysis of Soils and Minerals Using X-ray Absorption Spectroscopy. In *Mineralogical Methods*; Ulery, A. L.; Drees, L. R., Eds. Soil Science Society of America: Madison, WI,**2008**; Vol. Part 5, p 367.

[Crossref]

35. 35.

Bañuelos, G. S.; Fakra, S. C.; Walse, S. S.; Marcus, M. A.; Yang, S. I.; Pickering, I. J.; Pilon-Smits, E. A. H.;Freeman, J. L. Selenium Accumulation, Distribution, and Speciation in Spineless Prickly Pear Cactus: A Drought- and Salt-Tolerant, Selenium-Enriched Nutraceutical Fruit Crop for Biofortified Foods *Plant Physiol.***2011**, 155 (1) 315– 327 DOI: 10.1104/pp.110.162867

[Crossref], [PubMed], [CAS]

36. 36.

Newville, M. IFEFFIT: interactive XAFS analysis and FEFF fitting *J. Synchrotron Radiat.* **2001**, 8 (2) 322–324 DOI: 10.1107/S0909049500016964

[Crossref], [PubMed], [CAS]

37. 37.

Ravel, B.; Newville, M. ATHENA, ARTEMIS, HEPHAESTUS: data analysis for X-ray absorption spectroscopy using IFEFFIT *J. Synchrotron Radiat.* **2005**, 12 (4) 537– 541 DOI: 10.1107/S0909049505012719

[Crossref], [PubMed], [CAS]

38. 38.

Keller, R.; Holzapfel, W. B.; Schulz, H. Effect of pressure on the atom positions in Se and Te *Phys. Rev. B***1977**, 16 (10) 4404– 4412 DOI: 10.1103/PhysRevB.16.4404

[Crossref], [CAS]

39. 39.

Luef, B.; Fakra, S. C.; Csencsits, R.; Wrighton, K. C.; Williams, K. H.; Wilkins, M. J.; Downing, K. H.;Long, P. E.; Comolli, L. R.; Banfield, J. F. Iron-reducing bacteria accumulate ferric oxyhydroxide nanoparticle aggregates that may support planktonic growth *ISME J.* **2013**, 7 (2) 338– 350 DOI: 10.1038/ismej.2012.103

[Crossref], [PubMed], [CAS]

40. 40.

Grabovich, M.; Gavrish, E.; Kuever, J.; Lysenko, A. M.; Podkopaeva, D.; Dubinina, G. Proposal of Giesbergeria voronezhensis gen. nov., sp. nov. and G. kuznetsovii sp. nov. and reclassification of [Aquaspirillum] anulus, [A.] sinuosum and [A.] giesbergeri as Giesbergeria anulus comb. nov., G. sinuosa comb. nov. and G. giesbergeri comb. nov., and [Aquaspirillum] metamorphum and [A.] psychrophilum as Simplicispira metamorpha gen. nov., comb. nov. and S. psychrophila comb. nov *Int. J. Syst. Evol. Microbiol.***2006**, 56 (3) 569– 576

[PubMed], [CAS]

41. 41.

Yelton, A. P.; Williams, K. H.; Fournelle, J.; Wrighton, K. C.; Handley, K. M.; Banfield, J. F. Vanadate and Acetate Biostimulation of Contaminated Sediments Decreases Diversity, Selects for Specific Taxa, and Decreases Aqueous V5+ Concentration *Environ. Sci. Technol.* **2013**, 47 (12) 6500– 6509 DOI: 10.1021/es4006674

[ACS Full Text], [CAS]

42. 42.

Yelton, A. P. *Metagenomic and Cultivation-Based Analysis of Novel Microorganisms and Functions in Metal-Contaminated Environments*. UC Berkeley: Berkeley, CA, **2012**.

43. 43.

Zheng, S.; Su, J.; Wang, L.; Yao, R.; Wang, D.; Deng, Y.; Wang, R.; Wang, G.; Rensing, C. Selenite reduction by the obligate aerobic bacterium Comamonas testosteroni S44 isolated from a metal-contaminated soil *BMC Microbiol.* **2014**, 14, 204 DOI: 10.1186/s12866-014-0204-8

[Crossref], [PubMed], [CAS]

44. 44.

Willems, A.; Busse, J.; Goor, M.; Pot, B.; Falsen, E.; Jantzen, E.; Hoste, B.; Gillis, M.; Kersters, K.;Auling, G.; De Ley, J. Hydrogenophaga, a New Genus of Hydrogen-Oxidizing Bacteria That Includes Hydrogenophaga flava comb. nov. (Formerly Pseudomonas flava), Hydrogenophaga palleronii (Formerly Pseudomonas palleronii), Hydrogenophaga pseudoflava (Formerly Pseudomonas pseudoflava and “Pseudomonas carboxydoflava”), and Hydrogenophaga taeniospiralis (Formerly Pseudomonas taeniospiralis) *Int. J. Syst. Bacteriol.* **1989**, 39 (3) 319– 333 DOI: 10.1099/00207713-39-3-319

[Crossref], [CAS]

45. 45.

Lai, C.-Y.; Yang, X.; Tang, Y.; Rittmann, B. E.; Zhao, H.-P. Nitrate Shaped the Selenate-Reducing Microbial Community in a Hydrogen-Based Biofilm Reactor *Environ. Sci. Technol.* **2014**, 48 (6) 3395– 3402 DOI: 10.1021/es4053939

[ACS Full Text], [CAS]

46. 46.

Ranjard, L.; Prigent-Combaret, C.; Favre-Bonté, S.; Monnez, C.; Nazaret, S.; Cournoyer, B.Characterization of a novel selenium methyltransferase from freshwater bacteria showing strong similarities with the calicheamicin methyltransferase *Biochim. Biophys. Acta, Gene Struct. Expression* **2004**, 1679 (1)80– 85 DOI: 10.1016/j.bbaexp.2004.05.001

[Crossref], [PubMed], [CAS]

47. 47.

Dugan, P.; Stoner, D.; Pickrum, H., The Genus Zoogloea. In *The Prokaryotes*; Dworkin, M.; Falkow, S.;Rosenberg, E.; Schleifer, K.-H.; Stackebrandt, E., Eds. Springer: New York, **2006**; pp 960– 970.

[Crossref]

48. 48.

Srivastava, N.; Mukhopadhyay, M. Biosynthesis and structural characterization of selenium nanoparticles mediated by Zooglea ramigera *Powder Technol.* **2013**, 244 (0) 26– 29 DOI: 10.1016/j.powtec.2013.03.050

[Crossref], [CAS]

49. 49.

Cummings, D. E.; Caccavo, F., Jr.; Spring, S.; Rosenzweig, R. F. Ferribacterium limneticum, gen. nov., sp. nov., an Fe(III)-reducing microorganism isolated from mining-impacted freshwater lake sediments *Arch. Microbiol.* **1999**, 171 (3) 183– 188 DOI: 10.1007/s002030050697

[Crossref], [CAS]

50. 50.

Coates, J. D.; Chakraborty, R.; Lack, J. G.; O'Connor, S. M.; Cole, K. A.; Bender, K. S.; Achenbach, L. A.Anaerobic benzene oxidation coupled to nitrate reduction in pure culture by two strains of Dechloromonas*Nature* **2001**, 411 (6841) 1039– 1043 DOI: 10.1038/35082545

[Crossref], [PubMed], [CAS]

51. 51.

Zhang, Y.; Frankenberger, W. T., Jr. Supplementing Bacillus sp. RS1 with Dechloromonas sp. HZ for enhancing selenate reduction in agricultural drainage water *Sci. Total Environ.* **2007**, 372 (2–3) 397– 405DOI: 10.1016/j.scitotenv.2006.10.027

[Crossref], [PubMed], [CAS]

52. 52.

Chung, J.; Ryu, H.; Abbaszadegan, M.; Rittmann, B. E. Community structure and function in a H(2)-based membrane biofilm reactor capable of bioreduction of selenate and chromate *Appl. Microbiol. Biotechnol.***2006**, 72 (6) 1330– 1339 DOI: 10.1007/s00253-006-0439-x

[Crossref], [PubMed], [CAS]

53. 53.

Mouser, P. J.; N'Guessan, A. L.; Elifantz, H.; Holmes, D. E.; Williams, K. H.; Wilkins, M. J.; Long, P. E.;Lovley, D. R. Influence of Heterogeneous Ammonium Availability on Bacterial

Community Structure and the Expression of Nitrogen Fixation and Ammonium Transporter Genes during in Situ Bioremediation of Uranium-Contaminated Groundwater *Environ. Sci. Technol.* **2009**, 43 (12) 4386– 4392 DOI: 10.1021/es8031055

[ACS Full Text], [CAS]

54. 54.

N'Guessan, A. L.; Elifantz, H.; Nevin, K. P.; Mouser, P. J.; Methe, B.; Woodard, T. L.; Manley, K.;Williams, K. H.; Wilkins, M. J.; Larsen, J. T.; Long, P. E.; Lovley, D. R. Molecular analysis of phosphate limitation in Geobacteraceae during the bioremediation of a uranium-contaminated aquifer *ISME J.* **2010**, 4(2) 253– 266 DOI: 10.1038/ismej.2009.115

[Crossref], [PubMed], [CAS]

55. 55.

Handley, K. M.; Wrighton, K. C.; Piceno, Y. M.; Andersen, G. L.; DeSantis, T. Z.; Williams, K. H.;Wilkins, M. J.; N'Guessan, A. L.; Peacock, A.; Bargar, J.; Long, P. E.; Banfield, J. F. High-density PhyloChip profiling of stimulated aquifer microbial communities reveals a complex response to acetate amendment*FEMS Microbiol. Ecol.* **2012**, 81 (1) 188– 204 DOI: 10.1111/j.1574-6941.2012.01363.x

[Crossref], [PubMed], [CAS]

56. 56.

Wrighton, K. C.; Thomas, B. C.; Sharon, I.; Miller, C. S.; Castelle, C. J.; VerBerkmoes, N. C.; Wilkins, M. J.;Hettich, R. L.; Lipton, M. S.; Williams, K. H.; Long, P. E.; Banfield, J. F. Fermentation, Hydrogen, and Sulfur Metabolism in Multiple Uncultivated Bacterial Phyla *Science* **2012**, 337 (6102) 1661– 1665 DOI: 10.1126/science.1224041

[Crossref], [PubMed], [CAS]

57. 57.

Wrighton, K. C.; Castelle, C. J.; Wilkins, M. J.; Hug, L. A.; Sharon, I.; Thomas, B. C.; Handley, K. M.;Mullin, S. W.; Nicora, C. D.; Singh, A.; Lipton, M. S.; Long, P. E.; Williams, K. H.; Banfield, J. F. Metabolic interdependencies between phylogenetically novel fermenters and respiratory organisms in an unconfined aquifer *ISME J.* **2014**, 8 (7) 1452– 1463 DOI: 10.1038/ismej.2013.249

[Crossref], [PubMed], [CAS]

58. 58.

Handley, K. M.; VerBerkmoes, N. C.; Steefel, C. I.; Williams, K. H.; Sharon, I.; Miller, C. S.;Frischkorn, K. R.; Chourey, K.; Thomas, B. C.; Shah, M. B.; Long, P. E.; Hettich, R. L.; Banfield, J. F.Biostimulation induces syntrophic interactions that impact C, S and N cycling

in a sediment microbial community *ISME J.* **2013**, 7 (4) 800– 816 DOI: 10.1038/ismej.2012.148

[Crossref], [PubMed], [CAS]

59. 59.

Boyce, C. K.; Cody, G. D.; Feser, M.; Jacobsen, C.; Knoll, A. H.; Wirick, S. Organic chemical differentiation within fossil plant cell walls detected with X-ray spectromicroscopy *Geology* **2002**, 30 (11) 1039– 1042 DOI: 10.1130/0091-7613(2002)030<1039:OCDWFP>2.0.CO;2

[Crossref], [CAS]

60. 60.

Cody, G. D.; Ade, H.; Wirick, S.; Mitchell, G. D.; Davis, A. Determination of chemical-structural changes in vitrinite accompanying luminescence alteration using C-NEXAFS analysis *Org. Geochem.* **1998**, 28 (7–8)441– 455 DOI: 10.1016/S0146-6380(98)00010-2

[Crossref], [CAS]

61. 61.

Salinero, K.; Keller, K.; Feil, W.; Feil, H.; Trong, S.; Di Bartolo, G.; Lapidus, A. Metabolic analysis of the soil microbe Dechloromonas aromatica str. RCB: indications of a surprisingly complex life-style and cryptic anaerobic pathways for aromatic degradation *BMC Genomics* **2009**, 10 (1) 351 DOI: 10.1186/1471-2164-10-351

[Crossref], [PubMed], [CAS]

62. 62.

Yoon, S. C.; Choi, M. H. Local Sequence Dependence of Polyhydroxyalkanoic Acid Degradation in Hydrogenophaga pseudoflava *J. Biol. Chem.* **1999**, 274 (53) 37800– 37808 DOI: 10.1074/jbc.274.53.37800

[Crossref], [PubMed], [CAS]

63. 63.

Saito, T.; Saegusa, H.; Miyata, Y.; Fukui, T. Intracellular degradation of poly(3-hydroxybutyrate) granules of Zoogloea ramigera I-16-M *FEMS Microbiol. Lett.* **1992**, 103 (2–4) 333– 338 DOI: 10.1111/j.1574-6968.1992.tb05855.x

[Crossref]

64. 64.

Spring, S.; Wagner, M.; Schumann, P.; Kämpfer, P. Malikia granosa gen. nov., sp. nov., a novel polyhydroxyalkanoate- and polyphosphate-accumulating bacterium isolated from

activated sludge, and reclassification of Pseudomonas spinosa as Malikia spinosa comb. nov *Int. J. Syst. Evol. Microbiol.* **2005**, 55(2) 621– 629 DOI: 10.1099/ijs.0.63356-0

[Crossref], [PubMed], [CAS]

65. 65.

Madwid, J.; Andrahennadi, R.; Blyth, R.; Coulthard, I.; Doonan, C.J.; Liu, D.; Hoffmeyer, R.; Pu shie, M.J.;Regier, T.; Ruszkowski, J.; Singh, S.P.; Thavarajah, D.; Wiramanaden, C.I.E.; Yang, S.I.; Zhang, L.;George, G.N.; Pickering, I.J. *Selenium L-edge Spectroscopy at the SGM Beamline As a Tool for Environmental Selenium Speciation*; CLS: Cape Town, South Africa, **2008**.

66. 66.

Bugaris, D. E.; Copping, R.; Tyliszczak, T.; Shuh, D. K.; Ibers, J. A. La2U2Se9: An Ordered Lanthanide/Actinide Chalcogenide with a Novel Structure Type *Inorg. Chem.* **2010**, 49 (5) 2568– 2575 DOI: 10.1021/ic902503n

[ACS Full Text], [CAS]

67. 67.

Pickering, I. J.; Brown, G. E.; Tokunaga, T. K. Quantitative Speciation of Selenium in Soils Using X-ray Absorption Spectroscopy *Environ. Sci. Technol.* **1995**, 29 (9) 2456– 2459 DOI: 10.1021/es00009a043

[ACS Full Text], [CAS]

68. 68.

Ryser, A.; Strawn, D.; Marcus, M.; Johnson-Maynard, J.; Gunter, M.; Möller, G. Micro-spectroscopic investigation of selenium-bearing minerals from the Western US Phosphate Resource Area *Geochem. Trans.* **2005**, 6 (1) 1

[Crossref], [CAS]

69. 69.

Ryser, A. L.; Strawn, D. G.; Marcus, M. A.; Fakra, S.; Johnson-Maynard, J. L.; Möller, G. Microscopically Focused Synchrotron X-ray Investigation of Selenium Speciation in Soils Developing on Reclaimed Mine Lands *Environ. Sci. Technol.* **2006**, 40 (2) 462– 467 DOI: 10.1021/es051674i

[ACS Full Text], [CAS]

70. 70.

Sarret, G.; Avoscan, L.; Carrière, M.; Collins, R.; Geoffroy, N.; Carrot, F.; Covès, J.; Gouget, B. Chemical Forms of Selenium in the Metal-Resistant Bacterium Ralstonia metallidurans CH34

Exposed to Selenite and Selenate *Appl. Environ. Microbiol.* **2005**, 71 (5) 2331– 2337 DOI: 10.1128/AEM.71.5.2331-2337.2005

[Crossref], [PubMed], [CAS]

71. 71.

Majid, M.; Bénazeth, S.; Souleau, C.; Purans, J. XAFS study of interchain and intrachain order in Se1-xTex glasses: Nearest neighbors *Phys. Rev. B: Condens. Matter Mater. Phys.* **1998**, 58 (10) 6104– 6114 DOI: 10.1103/PhysRevB.58.6104

[Crossref], [CAS]

72. 72.

Yang, S. I.; Lawrence, J. R.; Swerhone, G. D. W.; Pickering, I. J. Biotransformation of selenium and arsenic in multi-species biofilm *Environ. Chem.* **2011**, 8 (6) 543– 551 DOI: 10.1071/EN11062

[Crossref], [CAS]

73. 73.

Minaev, V. S.; Timoshenkov, S. P.; Kalugin, V. V. Structural and phase transformations in condensed selenium *J. Optoelectron Adv. Mater.* **2005**, 7 (4) 1717– 1741

[CAS]

74. 74.

Herbel, M. J.; Blum, J. S.; Oremland, R. S.; Borglin, S. E. Reduction of Elemental Selenium to Selenide: Experiments with Anoxic Sediments and Bacteria that Respire Se-Oxyanions *Geomicrobiol. J.* **2003**, 20 (6)587– 602 DOI: 10.1080/713851163

[Crossref], [CAS]

75. 75.

Losi, M. E.; Frankenberger, W. T. Reduction of Selenium Oxyanions by *Enterobacter cloacae* SLD1a-1: Isolation and Growth of the Bacterium and Its Expulsion of Selenium Particles *Appl. Environ. Microbiol.***1997**, 63 (8) 3079– 84

[PubMed], [CAS]

76. 76.

Harrison, J. J.; Ceri, H.; Turner, R. J. Multimetal resistance and tolerance in microbial biofilms *Nat. Rev. Microbiol.* **2007**, 5 (12) 928– 938 DOI: 10.1038/nrmicro1774

[Crossref], [PubMed], [CAS]

77. 77.

Zehr, J. P.; Oremland, R. S. Reduction of Selenate to Selenide by Sulfate-Respiring Bacteria: Experiments with Cell Suspensions and Estuarine Sediments *Appl. Environ. Microbiol.* **1987**, 53 (6) 1365–1369

[PubMed], [CAS]

78. 78.

Oremland, R. S.; Blum, J. S.; Bindi, A. B.; Dowdle, P. R.; Herbel, M.; Stolz, J. F. Simultaneous Reduction of Nitrate and Selenate by Cell Suspensions of Selenium-Respiring Bacteria *Appl. Environ. Microbiol.* **1999**, 65(10) 4385– 4392

[PubMed], [CAS]

79. 79.

Steinberg, N. A.; Blum, J. S.; Hochstein, L.; Oremland, R. S. Nitrate Is a Preferred Electron Acceptor for Growth of Freshwater Selenate-Respiring Bacteria *Appl. Environ. Microbiol.* **1992**, 58 (1) 426–428

[PubMed], [CAS]

80. 80.

Dowdle, P. R.; Oremland, R. S. Microbial Oxidation of Elemental Selenium in Soil Slurries and Bacterial Cultures *Environ. Sci. Technol.* **1998**, 32 (23) 3749– 3755 DOI: 10.1021/es970940s

[ACS Full Text], [CAS]

81. 81.

Flemming, H. C.; Wingender, J. The biofilm matrix *Nat. Rev. Microbiol.* **2010**, 8 (9) 623– 33 DOI: 10.1038/nrmicro2415

[Crossref], [PubMed], [CAS]

82. 82.

Sutherland, I. W. The biofilm matrix – an immobilized but dynamic microbial environment *Trends Microbiol.***2001**, 9 (5) 222– 227 DOI: 10.1016/S0966-842X(01)02012-1

[Crossref], [PubMed], [CAS]

83. 83.

Dobias, J.; Suvorova, E. I.; Bernier-Latmani, R. Role of proteins in controlling selenium nanoparticle size*Nanotechnology* **2011**, 22 (19) 195605 DOI: 10.1088/0957-4484/22/19/195605

[Crossref], [PubMed], [CAS]

84. 84.

Kaur, G.; Iqbal, M.; Bakshi, M. S. Biomineralization of Fine Selenium Crystalline Rods and Amorphous Spheres *J. Phys. Chem. C* **2009**, 113 (31) 13670– 13676 DOI: 10.1021/jp903685g

[ACS Full Text], [CAS]

85. 85.

Pearce, C. I.; Pattrick, R. A. D.; Law, N.; Charnock, J. M.; Coker, V. S.; Fellowes, J. W.; Oremland, R. S.;Lloyd, J. R. Investigating different mechanisms for biogenic selenite transformations: Geobacter sulfurreducens, Shewanella oneidensis and Veillonella atypica *Environ. Technol.* **2009**, 30 (12) 1313– 1326DOI: 10.1080/09593330902984751

[Crossref], [PubMed], [CAS]

86. 86.

Lenz, M.; Kolvenbach, B.; Gygax, B.; Moes, S.; Corvini, P. F. Shedding light on selenium biomineralization: proteins associated with bionanominerals *Appl. Environ. Microbiol.* **2011**, 77 (13) 4676– 80 DOI: 10.1128/AEM.01713-10

[Crossref], [PubMed], [CAS]

87. 87.

Bayles, K. W. The biological role of death and lysis in biofilm development *Nat. Rev. Microbiol.* **2007**, 5 (9)721– 726 DOI: 10.1038/nrmicro1743

[Crossref], [PubMed], [CAS]

88. 88.

Buchs, B.; Evangelou, M. W. H.; Winkel, L. H. E.; Lenz, M. Colloidal Properties of Nanoparticular Biogenic Selenium Govern Environmental Fate and Bioremediation Effectiveness *Environ. Sci. Technol.* **2013**, 47 (5)2401– 2407 DOI: 10.1021/es304940s

[ACS Full Text], [CAS]

89. 89.

Moreau, J. W.; Weber, P. K.; Martin, M. C.; Gilbert, B.; Hutcheon, I. D.; Banfield, J. F. Extracellular Proteins Limit the Dispersal of Biogenic Nanoparticles *Science* **2007**, 316 (5831) 1600– 1603 DOI: 10.1126/science.1141064

[Crossref], [PubMed], [CAS]